

# UC Irvine

## UC Irvine Previously Published Works

### Title

Bright circularly polarized soft X-ray high harmonics for X-ray magnetic circular dichroism.

### Permalink

<https://escholarship.org/uc/item/0603r9tj>

### Journal

Proceedings of the National Academy of Sciences of the United States of America, 112(46)

### ISSN

0027-8424

### Authors

Fan, Tingting  
Grychtol, Patrik  
Knut, Ronny  
et al.

### Publication Date

2015-11-01

### DOI

10.1073/pnas.1519666112

Peer reviewed

# Bright circularly polarized soft X-ray high harmonics for X-ray magnetic circular dichroism

Tingting Fan<sup>a,1</sup>, Patrik Grychtol<sup>a</sup>, Ronny Knut<sup>a</sup>, Carlos Hernández-García<sup>a,b</sup>, Daniel D. Hickstein<sup>a</sup>, Dmitriy Zusin<sup>a</sup>, Christian Gentry<sup>a</sup>, Franklin J. Dollar<sup>a</sup>, Christopher A. Mancuso<sup>a</sup>, Craig W. Hogle<sup>a</sup>, Ofer Kfir<sup>c</sup>, Dominik Legut<sup>d,e</sup>, Karel Carva<sup>e,f</sup>, Jennifer L. Ellis<sup>a</sup>, Kevin M. Dorney<sup>a</sup>, Cong Chen<sup>a</sup>, Oleg G. Shpyrko<sup>g</sup>, Eric E. Fullerton<sup>h</sup>, Oren Cohen<sup>c</sup>, Peter M. Oppeneer<sup>f</sup>, Dejan B. Milošević<sup>i,j,k</sup>, Andreas Becker<sup>a</sup>, Agnieszka A. Jaroń-Becker<sup>a</sup>, Tenio Popmintchev<sup>a</sup>, Margaret M. Murnane<sup>a,1</sup>, and Henry C. Kapteyn<sup>a</sup>

<sup>a</sup>Department of Physics and JILA, University of Colorado, Boulder, CO 80309-0440; <sup>b</sup>Grupo de Investigación en Óptica Extrema, Universidad de Salamanca, Salamanca 37008, Spain; <sup>c</sup>Solid State Institute and Physics Department, Technion, Haifa 32000, Israel; <sup>d</sup>IT4Innovations Center, VSB Technical University of Ostrava, CZ 708 33 Ostrava, Czech Republic; <sup>e</sup>Faculty of Mathematics and Physics, Department of Condensed Matter Physics, Charles University in Prague, CZ-12116 Prague 2, Czech Republic; <sup>f</sup>Department of Physics and Astronomy, Uppsala University, 75120 Uppsala, Sweden; <sup>g</sup>Department of Physics, University of California San Diego, La Jolla, CA 92093; <sup>h</sup>Center for Magnetic Recording Research, University of California San Diego, La Jolla, CA 92093-0401; <sup>i</sup>Faculty of Science, University of Sarajevo, 71000 Sarajevo, Bosnia and Herzegovina; <sup>j</sup>Academy of Sciences and Arts of Bosnia and Herzegovina, 71000 Sarajevo, Bosnia and Herzegovina; and <sup>k</sup>Max-Born-Institut, 12489 Berlin, Germany

Contributed by Margaret M. Murnane, October 6, 2015 (sent for review September 19, 2015); reviewed by Jean-Yves Bigot and Yuen-Ron Shen

**We demonstrate, to our knowledge, the first bright circularly polarized high-harmonic beams in the soft X-ray region of the electromagnetic spectrum, and use them to implement X-ray magnetic circular dichroism measurements in a tabletop-scale setup. Using counterrotating circularly polarized laser fields at 1.3 and 0.79  $\mu\text{m}$ , we generate circularly polarized harmonics with photon energies exceeding 160 eV. The harmonic spectra emerge as a sequence of closely spaced pairs of left and right circularly polarized peaks, with energies determined by conservation of energy and spin angular momentum. We explain the single-atom and macroscopic physics by identifying the dominant electron quantum trajectories and optimal phase-matching conditions. The first advanced phase-matched propagation simulations for circularly polarized harmonics reveal the influence of the finite phase-matching temporal window on the spectrum, as well as the unique polarization-shaped attosecond pulse train. Finally, we use, to our knowledge, the first tabletop X-ray magnetic circular dichroism measurements at the  $N_{4,5}$  absorption edges of Gd to validate the high degree of circularity, brightness, and stability of this light source. These results demonstrate the feasibility of manipulating the polarization, spectrum, and temporal shape of high harmonics in the soft X-ray region by manipulating the driving laser waveform.**

X-rays | high harmonics generation | magnetic material | ultrafast light science | phase matching

High-harmonic generation (HHG) results from an extreme nonlinear quantum response of atoms to intense laser fields. When implemented in a phase-matched geometry, bright, coherent HHG beams can extend to photon energies beyond 1.6 keV (1, 2). For many years, however, bright HHG was limited to linear polarization, precluding many applications in probing and characterizing magnetic materials and nanostructures, as well as chiral phenomena in general. Although X-ray optics can in principle be used to convert extreme UV (EUV) and X-ray light from linear to circular polarization, in practice such optics are challenging to fabricate and have poor throughput and limited bandwidth (3). A more appealing option is the direct generation of elliptically polarized (4–6) and circularly polarized (7–9) high harmonics. In recent work we showed that by using a combination of 0.8 and 0.4  $\mu\text{m}$  counterrotating driving fields, bright (i.e., phase-matched) EUV HHG with circular polarization can be generated at wavelengths  $\lambda > 18$  nm and used for EUV magnetic dichroism measurements (10–13).

Here we make, to our knowledge, the first experimental demonstration of circularly polarized harmonics in the soft X-ray region to wavelengths  $\lambda < 8$  nm, and use them to implement soft X-ray magnetic circular dichroism (XMCD) measurements using a tabletop-scale setup. By using counterrotating driving lasers at

0.79  $\mu\text{m}$  (1.57 eV) and 1.3  $\mu\text{m}$  (0.95 eV), we generate bright circularly polarized soft X-ray HHG beams with photon energies greater than 160 eV (14) and with flux comparable to the HHG flux obtained using linearly polarized 800-nm driving lasers (15). Moreover we implement, to our knowledge, the first advanced simulations of the coherent buildup of circularly polarized high harmonics to show how the macroscopic phase-matching physics and ellipticity of the driving lasers influence the HHG spectra, number of bright attosecond bursts, and the degree of circular polarization.

This work presents several new capabilities and findings. First, circularly polarized HHG provides a unique route for generating bright narrowband ( $\lambda/\Delta\lambda > 400$ ) harmonic peaks in the soft X-ray region, to complement the soft X-ray supercontinua that are produced with linearly polarized mid-IR lasers (2, 15, 16). This capability is significant because it provides an elegant and efficient route for shaping soft X-ray light by manipulating the driving laser light, and is very useful for applications in high-resolution coherent imaging (17–21) and photoelectron spectroscopies. Second, we show that the macroscopic phase-matching physics of circularly

## Significance

**The new ability to generate circularly polarized coherent (laser-like) beams of short wavelength high harmonics in a tabletop-scale setup is attracting intense interest worldwide. Although predicted in 1995, this capability was demonstrated experimentally only in 2014. However, all work to date (both theory and experiment) studied circularly polarized harmonics only in the extreme UV (EUV) region of the spectrum at wavelengths  $> 18$  nm. In this new work done in a broad international collaboration, we demonstrate the first soft X-ray high harmonics with circular polarization to wavelengths  $\lambda < 8$  nm and the first tabletop soft X-ray magnetic circular dichroism (XMCD) measurements, and also uncover new X-ray light science that will inspire many more studies of circular high-harmonic generation (HHG).**

Author contributions: T.F., M.M.M., and H.C.K. designed research; T.F., P.G., R.K., D.D.H., D.Z., C.G., F.J.D., C.A.M., C.W.H., J.L.E., K.M.D., C.C., and T.P. performed research; C.H.-G., D.L., K.C., O.G.S., E.E.F., P.M.O., D.B.M., A.B., and A.A.J.-B. contributed new reagents/analytic tools; T.F., P.G., R.K., and M.M.M. analyzed data; T.F., P.G., R.K., C.H.-G., D.D.H., O.K., O.C., T.P., M.M.M., and H.C.K. wrote the paper.

Reviewers: J.-Y.B., Université de Strasbourg; and Y.-R.S., University of California, Berkeley. The authors declare no conflict of interest.

Freely available online through the PNAS open access option.

<sup>1</sup>To whom correspondence may be addressed. Email: murnane@jila.colorado.edu or tingting.fan@colorado.edu.

This article contains supporting information online at [www.pnas.org/lookup/suppl/doi:10.1073/pnas.1519666112/-DCSupplemental](http://www.pnas.org/lookup/suppl/doi:10.1073/pnas.1519666112/-DCSupplemental).

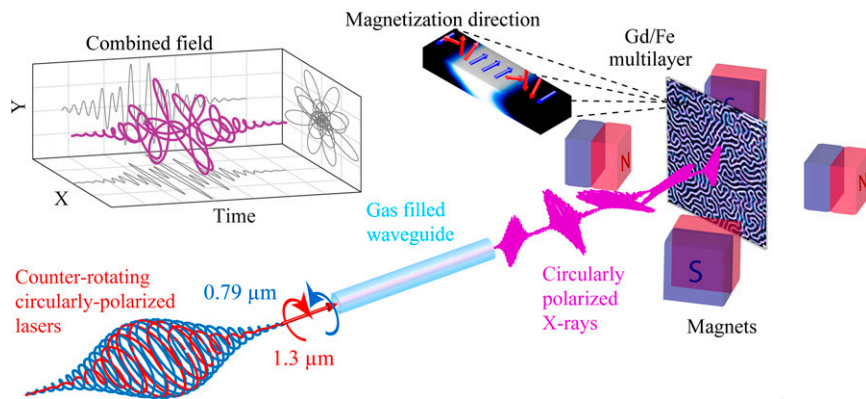


**Fig. 1.** Experimental scheme. Bright, circularly polarized, soft X-ray beams were generated by focusing 0.79- and 1.3- $\mu\text{m}$  counterrotating circularly polarized laser fields into a gas-filled waveguide; they are then used for XMCD measurements at the  $N_{4,5}$  absorption edges of Gd as well as the  $M_{2,3}$  absorption edge of Fe from an out-of-plane magnetized Gd/Fe multilayer sample. (*Left Inset*) Combined field of the two drivers.

polarized soft X-ray HHG driven by mid-IR lasers has similarities to linearly polarized HHG, where the number of bright attosecond bursts is limited by the finite phase-matching temporal window. Third, we implement the first tabletop XMCD measurements at the  $N_{4,5}$  absorption edges of Gd. The Gd/Fe multilayer sample is a candidate material for next-generation all-optical magnetic storage devices (22), but has been inaccessible to HHG XMCD until now. This capability also opens up the possibility of probing spin dynamics in rare-earth elements using HHG, which has been successfully used for 3d transition metals to uncover the fastest spin dynamics using EUV HHG (23, 24). Finally, and most importantly, these results demonstrate the universal nature of circularly polarized HHG that can be generated across the EUV and soft X-ray spectral regions using a broad range of driving laser wavelengths.

### Experiment

In our experiment, we used a single-stage Ti:sapphire regenerative amplifier with an output energy of 8.2 mJ per pulse, at a 1-kHz repetition rate and a 0.79- $\mu\text{m}$  central wavelength (15). Approximately 80% of the output energy is directed into a three-stage

optical parametric amplifier (OPA) that generates a 1.6-mJ/pulse signal beam at 1.3  $\mu\text{m}$ , as well as a 1-mJ/pulse idler beam at 2  $\mu\text{m}$ . The polarizations of the signal beam and the remaining 20% of the 0.79- $\mu\text{m}$  beam are then converted to counterrotating circular polarization using half- and quarter-wave plates. A delay line is used for adjusting the relative time delay between the two fields. Both beams are then combined by a dichroic mirror and focused into a 150- $\mu\text{m}$  diameter, 1-cm long gas-filled hollow waveguide. The pulse durations of the 0.79- and 1.3- $\mu\text{m}$  beams are  $\sim 55$  and  $\sim 35$  fs, respectively. As illustrated schematically in Fig. 1, the counterrotating bichromatic drivers interact with a noble gas inside the fiber, generating circularly polarized high harmonics that propagate through a spectrometer and are recorded by a CCD. After the fiber, the two driving lasers are blocked using either a 0.4- $\mu\text{m}$  Al or 0.4- $\mu\text{m}$  Zr filter, which transmit in the range of 20–72 eV and 70–190 eV (25), respectively.

For our first set of experiments, we filled the waveguide with Ar, Ne, or He gas. As shown in Fig. 2, all HHG spectra exhibit a well-separated HHG peak-pair structure, where the harmonics within each pair possess opposite helicity. The HHG spectra from Ar and Ne terminate slightly above 50 and 120 eV,

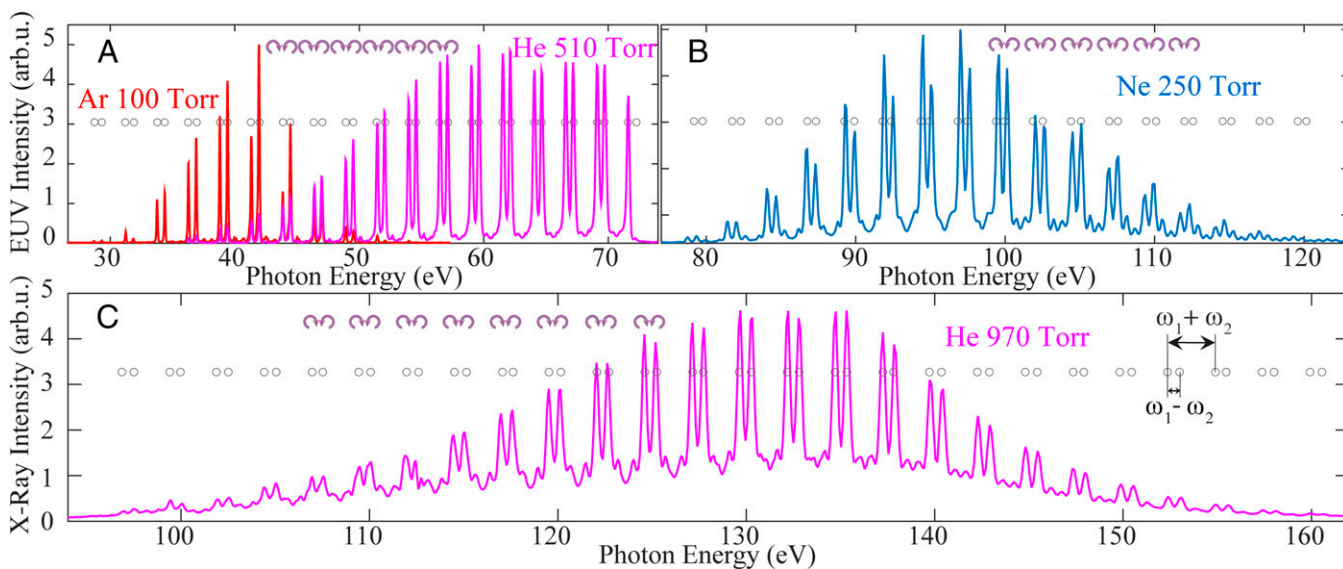


**Fig. 2.** Circularly polarized EUV and soft X-ray HHG. Experimental HHG spectra generated from Ar (A), Ne (B), and He (A and C) driven by counterrotating 0.79- and 1.3- $\mu\text{m}$  laser fields. All spectra show a peak-pair structure, located at positions predicted by energy and spin angular momentum conservation (circles). The separation within each pair is  $\omega_1 - \omega_2$ , and different pairs are separated by  $\omega_1 + \omega_2$ .



respectively, whereas for He, bright circularly polarized HHG extends dramatically beyond the previous limit of 70 to >160 eV (11). Moreover, circular HHG driven by 0.79- and 1.3- $\mu\text{m}$  lasers covers a much broader spectrum compared with circular HHG driven by 0.8  $\mu\text{m}$  and its second harmonic (11). This behavior is similar to the case for linearly polarized HHG, where long wavelength lasers generate the broadest HHG spectrum and can support the shortest transform-limited HHG pulse durations. Finally, the soft X-ray HHG spectra from Ne, and especially He, appear to merge into an underlying supercontinuum, which, as discussed below, is a result of peak broadening caused by the narrow phase-matching temporal window ( $\sim 8$  fs) (26), combined with additional peaks induced by slightly elliptical ( $\sim 0.99$ ) broadband driving lasers (10, 27, 28).

We can describe the experimentally observed HHG spectra in terms of the conservation of energy and photon-spin angular momentum (1, 8, 10, 27, 28). Conservation of energy gives  $\omega_c = n\omega_1 + l\omega_2$  for the circular harmonic  $\omega_c$  generated from  $n$  photons of frequency  $\omega_1$  and  $l$  photons of frequency  $\omega_2$ . Spin angular momentum conservation for generating circular polarization requires  $l = n \pm 1$ . Thus,  $\omega_c = n\omega_1 + (n \pm 1)\omega_2$ ; this gives rise to pairs of adjacent harmonics with opposite circular polarizations, and with a photon energy difference of  $\omega_1 - \omega_2$  between the harmonics within each pair, and  $\omega_1 + \omega_2$  between adjacent pairs. If we define  $\omega_1 = q\omega_2$ , where  $q$  can be any number, we obtain  $\omega_c = n(q + 1)\omega_2 \pm \omega_2$ . For the simple case of HHG driven by  $\omega$  and  $2\omega$ , where  $\omega_1 = 2\omega_2$ , it follows that  $\omega_c = (3n \pm 1)\omega_2$ , thereby resulting in a unique spectrum where every third harmonic order is missing. For the driving laser wavelengths studied here (0.79 and 1.3  $\mu\text{m}$ ),  $\omega_c \sim (2.65n \pm 1)\omega_2$ . As Fig. 2 shows, the experimentally generated HHG peak positions well match those predicted by the selection rules.

### Discussion

We performed microscopic and macroscopic simulations for circular HHG from He to unveil the physics underlying this unique soft X-ray HHG source. For our first simulation, we identified the relevant quantum trajectories using the strong-field approximation and quantum orbit theory (29) and applying the corresponding semiclassical three-step model (30–32). For simplification, our microscopic simulations were done at a central wavelength of 0.78  $\mu\text{m}$  (close to the 0.79- $\mu\text{m}$  experimental value), because for driving wavelengths of 1.3 and 0.78  $\mu\text{m}$ , the combined field (Fig. 3B) repeats itself in an eightfold symmetry shape every 13 fs (see *SI Text, Circularly Polarized HHG Driven by Bichromatic Counterrotating Fields*, for more information). Fig. 3A shows the dominant electron trajectories for a photon energy of 100 eV (see *SI Text, Single-Atom Simulations of the Electron Trajectories in Circular HHG*, for more information). In general, the electron tunnels a few atomic units away from the nucleus (33) and moves on a simple out-and-back trajectory, before recombining and emitting a harmonic photon. Ionization, recollision, and HHG occur eight times, each 13 fs, as shown in Fig. 3B. As a result, the HHG emission emerges as a series of eight linearly polarized attosecond bursts every 13 fs, with each burst rotated with respect to the previous one, until the amplitude of the laser field drops below the threshold for HHG. Note that the linear polarization results from the sum of counterrotating circularly polarized harmonics (34).

To fully explain the HHG spectra and its polarization state, including the underlying supercontinuum structure observed in the soft X-ray region in Fig. 2C, we need to consider circularly polarized HHG phase-matched propagation as well as the ellipticity of the driving lasers; to achieve this, we simulated the macroscopic phase matched buildup of a circularly polarized HHG field by computing 1D propagation through 2 mm He gas (300 torr), using the electromagnetic field propagator (35) (see *SI Text, Temporal Phase-Matching of Circularly Polarized Soft X-ray Harmonics*,

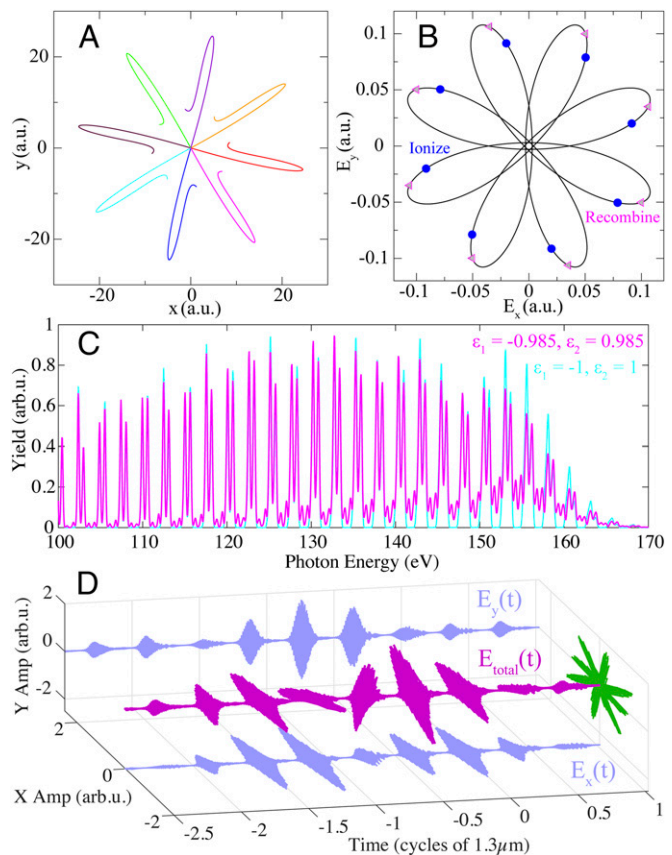


**Fig. 3.** Simulations of circularly polarized soft X-ray HHG from He. (A) Dominant electron trajectories for counterrotating lasers that result in the emission of a 100-eV photon. (B) Laser wavelengths of 1.3 and 0.78  $\mu\text{m}$  generate an eightfold symmetric field, where the ionization (circles) and recombination (triangles) times for the trajectories in A are indicated. (C) Simulated HHG spectra after macroscopic propagation for counterrotating laser drivers with perfect circularity ( $\epsilon_1 = -1, \epsilon_2 = 1$ , cyan) and slight ellipticity ( $\epsilon_1 = -0.985, \epsilon_2 = 0.985$ , magenta). Additional peaks appear when a slight ellipticity is introduced. (D) Attosecond pulse trains [ $E_x(t), E_y(t)$ , and  $E_{\text{total}}(t)$ ] obtained by performing a Fourier transform of the magenta spectrum in C shows a short phase-matching temporal window limits bright HHG to 5-attosecond bursts, with 2.6 linearly polarized bursts per 1.3- $\mu\text{m}$  cycle.

for details). This simulation was performed at driving laser intensities of  $I_1 = 2.40 \times 10^{14} \text{ W/cm}^2$  and  $I_2 = 2.20 \times 10^{14} \text{ W/cm}^2$ , chosen to fulfill the optimal phase-matching conditions, i.e., the sum of the phase mismatches for the two colors is zero slightly before the peak of the pulse, at an ionization level between the critical ionization for the two laser wavelengths (1). This choice also yields good agreement between the experimental and theoretical HHG spectra. In Fig. 3C (cyan curve), we present the propagated HHG spectrum for counterrotating driving laser fields with perfect circularity ( $\epsilon_1 = -1, \epsilon_2 = 1$ ).

However, the presence of small side-peaks adjacent to the main peaks in Fig. 2B and C provides a clue that additional channels are opening up, which can be explained using a simple photon model (10, 27, 28). In the presence of a slight ellipticity in one or both of the driving lasers, photons of the wrong helicity may be absorbed, leading to small peaks with different helicities underlying and surrounding each main peak (*SI Text, Imperfect Circularity of the Driving Laser Fields Introduces New HHG Channels*). This simple photon model can be used to explain the experimentally observed spectrum and also allows the ellipticity of the HHG spectrum to be extracted. The circularity of the HHG reduces from  $\sim 1$  in the EUV to  $\sim 0.6$  in the soft X-ray region (*SI Text, Ellipticity Analysis of*

*Circularly Polarized HHG Using Simple and Advanced Models*). However, each HHG peak will be perfectly circularly polarized if the driving lasers are perfectly circularly polarized.

To reproduce the underlying supercontinuum structure in the advanced macroscopic propagation simulations, we introduce a slight ellipticity into the driving laser pulses ( $\epsilon_1 = -0.985, \epsilon_2 = 0.985$ ) in Fig. 3C (magenta curve), which can be expected because of the finite bandwidth of zero-order wave plates. New low-intensity harmonic peaks appear because additional new channels are allowed (10, 27, 28) (*SI Text, Imperfect Circularity of the Driving Laser Fields Introduces New HHG Channels*), which when combined with peak broadening that results from a short temporal phase-matching window, can reproduce the supercontinuum structure, in excellent agreement with experiment.

In Fig. 3D, we present the predicted HHG emission in the temporal domain obtained by performing a Fourier transform of the magenta spectrum shown in Fig. 3C. The attosecond pulse train has circular polarization when either left or right circular HHG orders are considered separately (34, 36). When all HHG orders (left and right circular) are combined, a linearly polarized attosecond pulse train is generated, with subsequent bursts oriented in different directions and separated by (13/8) fs or 1.63 fs (because there are eight bursts each 13 fs). Similar to the case for soft X-ray HHG driven by linearly polarized mid-IR driving lasers, circularly polarized soft X-ray HHG optimally phase matches (26, 37) (i.e., is brightest at the highest photon energies)

at high gas pressures. Fig. 3D and *SI Text, Temporal Phase-Matching of Circularly Polarized Soft X-ray Harmonics* show that for these pressures and wavelengths, the temporal window for bright phase-matched HHG emission is considerably narrower than at shorter laser wavelengths (26); as a consequence, only five bright attosecond bursts are emitted, and the harmonic peaks broaden in the spectral domain. If the phase-matching window closes further, an isolated linearly polarized pulse or a circularly polarized pulse would be obtained if harmonics from both polarization states or from just one polarization state are selected, respectively. In comparison, when HHG is driven by linearly polarized mid-IR lasers, phase matching can isolate a single attosecond burst, and a supercontinuum of linearly polarized HHG is obtained (26).

Finally, we note that a unique aspect of circularly polarized HHG is its very high stability, as validated by the XMCD measurements (*SI Text, XMCD Shows the Brightness and Stability of Soft X-ray Circular HHG*), because the shape of the combined driving laser field is largely insensitive to phase slip between the two driving lasers. Rather, the combined field will simply rotate (11), which makes circular HHG highly stable—even if the two drivers are not phase locked—and thus very attractive for applications.

XMCD measurements can serve both to spectrally characterize the polarization of a light source, and to make fundamental materials measurements. Here, we use an out-of-plane magnetized Gd/Fe multilayer sample to perform XMCD at the

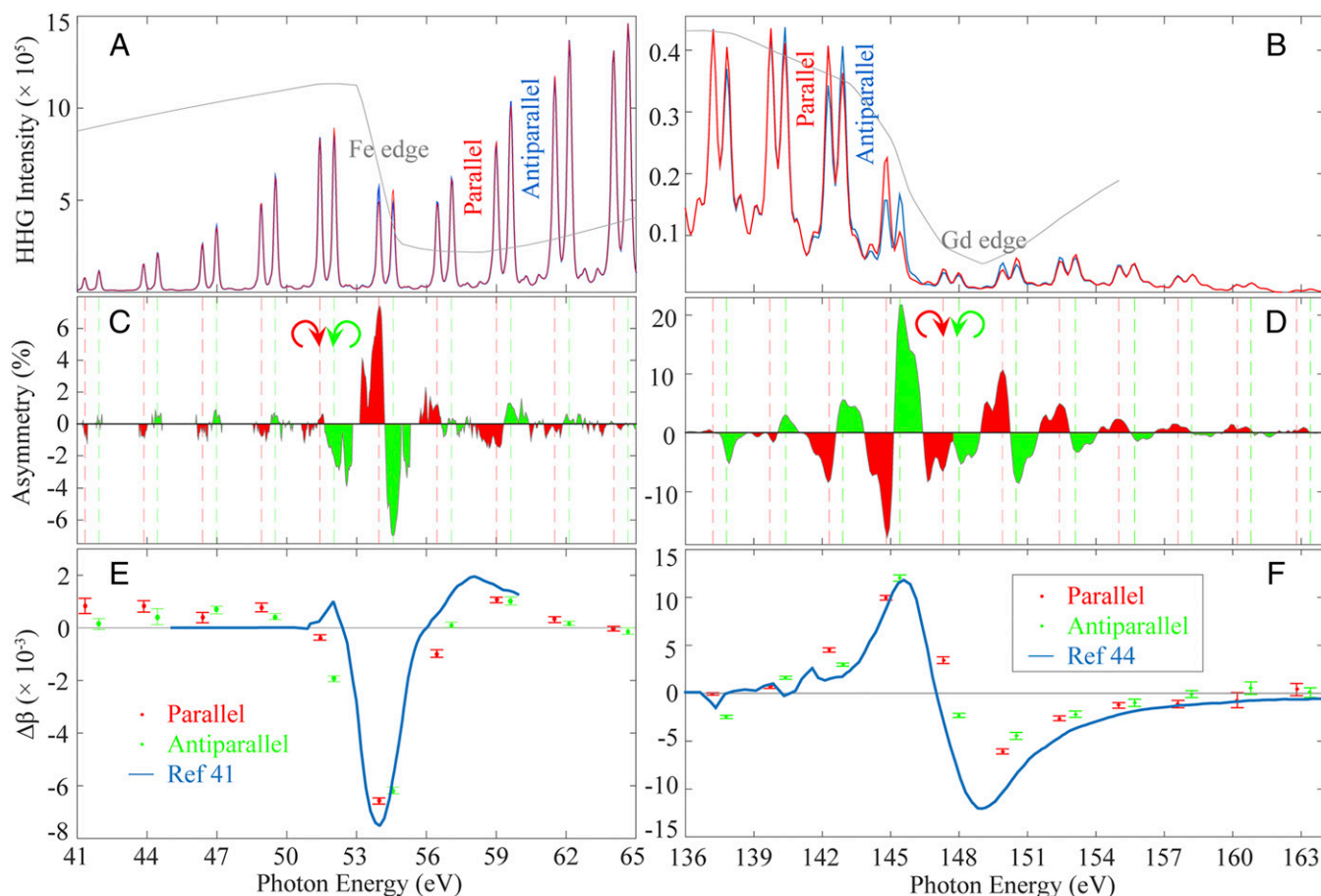


**Fig. 4.** EUV and X-ray magnetic circular dichroism of Fe and Gd. (A and B) HHG spectra around the Fe  $M_{2,3}$  and Gd  $N_{4,5}$  edges, transmitted through a Gd/Fe multilayer as the magnetization direction is parallel (red) and antiparallel (blue) to the HHG propagation direction. Gray curves, transmission of Fe and Gd. (C and D) XMCD asymmetry of Fe and Gd, with opposite signs for left (green) and right (red) circularly polarized HHG demonstrating opposite circularity of adjacent harmonics. (E and F) Extracted MO absorption coefficients at the Fe  $M_{2,3}$  and the Gd  $N_{4,5}$  edges (after correcting for ellipticity) agree well with literature values (41, 43, 44) (see *SI Text, XMCD Shows the Brightness and Stability of Soft X-ray Circular HHG*, for details).



$N_{4,5}$  absorption edges of the rare-earth metal Gd around 145 eV, as well as at the Fe  $M_{2,3}$  absorption edges around 54 eV. The observed magnetic contrast confirms that our soft X-ray HHG beams indeed exhibit circular polarization and are bright enough for applications. As schematically depicted in Fig. 1, the Gd/Fe multilayer sample is surrounded by four permanent (NdFeB) magnets (6), which provide a magnetic field perpendicular to the sample.

The transmitted intensity  $I^\pm = I_0 e^{-2\omega d \text{Im}(n_\pm)/c}$  of a circularly polarized HHG beam with incident intensity  $I_0$ , through the sample with thickness  $d$ , was recorded with the magnetic field both parallel ( $I^+$ ) and antiparallel ( $I^-$ ) to the wave vector ( $\mathbf{k}$ ) of the X-rays with energy  $\hbar\omega$ . The refractive index is defined as  $n_\pm = 1 - (\delta \pm \Delta\delta) + i(\beta \pm \Delta\beta)$ , where  $\beta$  and  $\Delta\beta$  are the absorptive index and its magneto-optical (MO) correction, respectively (38–40). From  $I^\pm$  we obtain the XMCD asymmetry, defined as  $A_{XMCD} = (I^+ - I^-)/(I^+ + I^-) = -\tanh(2\omega d \Delta\beta/c)$ , from which the MO absorption coefficient  $\Delta\beta = \Re(\epsilon_{xy}/2/\sqrt{\epsilon_{xx}})$  is extracted and compared with previous synchrotron work (41–46), with  $\epsilon_{ij}$  representing different components of the dielectric tensor. Note that the opposite sign of  $A_{XMCD}$  for adjacent harmonics (Fig. 4) demonstrates that they have opposite helicities.

By analyzing the strong XMCD signal, we extracted the MO absorption constant across a broad photon energy range above and below the Gd and Fe edges. As can be seen from Fig. 4, the excellent agreement between the extracted MO absorption coefficients and previous work (41, 44) shows that HHG can be successfully used for tabletop XMCD. The MO constants of Fe and Gd around the absorption edges show opposite signs. Because  $\Delta\beta$  has the same sign for both elements (41, 44), this indicates an antiferromagnetic alignment between Fe and Gd layers, as expected for these multilayers (47). Moreover, the XMCD results show that the small side peaks, which result from the imperfect circularity of the driving fields, also exhibit a high degree of circularity with the same circular polarization as their nearest main harmonic peak. Our results demonstrate the brightness, stability, and high degree of circularity of the generated harmonics, which extends element-specific and magnetic-sensitive ultrafast pump-probe capabilities into the soft X-ray range and to the 4f rare earth ferromagnets, with potential to reach the  $L$  shell absorption edges of many magnetic materials in the keV range in the near future (2).

In summary, using circularly polarized, counterrotating, bichromatic 0.79- and 1.3- $\mu\text{m}$  driving lasers, we demonstrated, to our knowledge, the first bright, phase-matched, soft X-ray HHG with circular polarization. The unique harmonic spectrum is explained by the microscopic and macroscopic physics of the generation process i.e., energy and spin angular momentum conservation laws, the driving laser wavelengths and degree of circular polarization, as well as the phase-matching conditions. This powerful new light source allowed us to perform what we believe is

the first tabletop soft X-ray magnetic circular dichroism measurements at the  $N_{4,5}$  absorption edges ( $\sim 145$  eV) of the technologically important rare earth metal Gd. Such materials are of wide interest because they are potentially important for next-generation data storage media using all-optical switching, and were inaccessible to investigation via tabletop HHG until now. Finally, this work demonstrates that circular HHG can be implemented across a broad range of photon energies, enhancing our ability to control X-ray light using laser light, and provides a breakthrough tool for probing ultrafast magnetization dynamics using tabletop soft X-rays.

## Methods

Here, we present the details of the XMCD measurement. As shown in Fig. 1, the four permanent magnets are mounted on a rotation stage such that their generated magnetic field could be applied perpendicular to the sample surface in either direction. The magnetic contrast is obtained by switching the magnetic field between parallel/antiparallel alignment relative to the HHG propagation vector. The external magnetic field  $\mu_0 H$  at the sample was 230 mT, measured with a Hall probe—high enough to saturate the magnetization of the multilayer sample (48) as confirmed by vibrating sample magnetometry. The out-of-plane magnetized multilayer sample, which consists of 50 repetitions of Gd (0.45 nm)/Fe (0.41 nm) layer pairs, was deposited on a 50-nm  $\text{Si}_3\text{N}_4$  membrane to enable a transmission geometry, and capped by 3 nm of Ta to prevent oxidation. For the XMCD measurements, we used the harmonics generated in He with 1.3- and 0.79- $\mu\text{m}$  drivers, where the laser peak intensities and the gas pressure were optimized for phase matching at the higher and lower energy parts of the spectrum, corresponding to the Gd and Fe absorption edges, respectively (Fig. 2 A and C). Because the phase mismatch becomes larger with broader bandwidth (11, 34), we were not able to phase match the entire spectrum at the same time. In addition, for Ar and He circular HHG spectra in Fig. 2 A and C and the XMCD measurement in Fig. 4, the CCD used is Andor Newton DO940P-BN; for Ne circular HHG spectra in Fig. 2B, the CCD used is Andor DO420-BN.

**ACKNOWLEDGMENTS.** The authors thank Wilhelm Becker and Luis Plaja for useful discussions. Support for this work was provided by the Department of Energy (DOE) Office of Basic Energy Sciences X-Ray Scattering Program and the National Science Foundation (NSF) Physics Frontier Center Program Grant PHY-1125844 (to T.F., P.G., R.K., D.D.H., D.Z., C.G., F.J.D., C.A.M., C.W.H., J.L.E., K.M.D., C.C., T.P., A.B., H.C.K. and M.M.M.); NSF Graduate Research Fellowship DGE-1144083 (to J.L.E.); Marie Curie International Outgoing Fellowship within the European Union (EU) Seventh Framework Program for Research and Technological Development (2007–2013), under REA Grant 328334 (to C.H.-G.); Junta de Castilla y León Project SA116U13, UIC016 (to C.H.-G.); MINECO Grant FIS2013-44174-P (to C.H.-G.); US NSF Grants PHY-1125844 and PHY-1068706 (to A.A.J.-B.); Deutsche Forschungsgemeinschaft Grant GR 4234/1-1 (to P.G.); Swedish Research Council (R.K. and P.M.O.); EU Seventh Framework Programme Grant 281043, FemtoSpin (to K.C. and P.M.O.); Czech Science Foundation Grant 15-08740Y (to K.C.); IT4Innovations Centre of Excellence Project CZ.1.05/1.1.00/02.0070 funded by the European Regional Development Fund and the national budget of the Czech Republic Project Large Research, Development and Innovations Infrastructures LM2011033 (to D.L.); US DOE, Office of Science, Office of Basic Energy Sciences Contract DE-SC0001805 (to O.G.S.); and US DOE Office of Basic Energy Sciences Award DE-SC0003678 (to E.E.F.). This work used the Janus supercomputer, which is supported by US NSF Award CNS-0821794 and the University of Colorado, Boulder.

- Rundquist A, et al. (1998) Phase-matched generation of coherent soft X-rays. *Science* 280(5368):1412–1415.
- Popmintchev T, et al. (2012) Bright coherent ultrahigh harmonics in the keV x-ray regime from mid-infrared femtosecond lasers. *Science* 336(6086):1287–1291.
- Vodungbo B, et al. (2011) Polarization control of high order harmonics in the EUV photon energy range. *Opt Express* 19(5):4346–4356.
- Zhou X, et al. (2009) Elliptically polarized high-order harmonic emission from molecules in linearly polarized laser fields. *Phys Rev Lett* 102(7):073902.
- Ferré A, et al. (2014) A table-top ultrashort light source in the extreme ultraviolet for circular dichroism experiments. *Nat Photonics* 9:93–98.
- Lambert G, et al. (2015) Towards enabling femtosecond helicity-dependent spectroscopy with high-harmonic sources. *Nat Commun* 6:6167.
- Eichmann H, et al. (1995) Polarization-dependent high-order two-color mixing. *Phys Rev A* 51(5):R3414–R3417.
- Long S, Becker W, McIver JK (1995) Model calculations of polarization-dependent two-color high-harmonic generation. *Phys Rev A* 52(3):2262–2278.
- Tong XM, Chu SI (1998) Generation of circularly polarized multiple high-order harmonic emission from two-color crossed laser beams. *Phys Rev A* 58:2656–2659.
- Fleischer A, Kfir O, Diskin T, Sidorenko P, Cohen O (2014) Spin angular momentum and tunable polarization in high-harmonic generation. *Nat Photonics* 8:543–549.
- Kfir O, et al. (2015) Generation of bright phase-matched circularly-polarized extreme ultraviolet high harmonics. *Nat Photonics* 9:99–105.
- Grychtol P, et al. (2015) X-ray magnetic circular dichroism probed using high harmonics. *Ultrafast Phenomena XIX*, eds Yamanouchi K, et al. Springer Proceedings in Physics (Springer, New York), pp 60–77.
- Hickstein DD, et al. (2015) Noncollinear generation of angularly isolated circularly polarized high harmonics. *Nat Photonics*, 10.1038/nphoton.2015.181.
- Fan T, et al. (2015) Bright circularly polarized soft X-ray high harmonics for X-ray magnetic circular dichroism. *CLEO: 2015 Postdeadline Paper Digest* (Optical Soc of America, Washington, DC), JTh5C.1.
- Ding C, et al. (2014) High flux coherent super-continuum soft X-ray source driven by a single-stage, 10mJ, Ti:sapphire amplifier-pumped OPA. *Opt Express* 22(5):6194–6202.
- Chen MC, et al. (2010) Bright, coherent, ultrafast soft X-ray harmonics spanning the water window from a tabletop light source. *Phys Rev Lett* 105(17):173901.
- Zhang B, et al. (2013) Full field tabletop EUV coherent diffractive imaging in a transmission geometry. *Opt Express* 21(19):21970–21980.

18. Zhang B, et al. (2015) High contrast 3D imaging of surfaces near the wavelength limit using tabletop EUV ptychography. *Ultramicroscopy* 158:98–104.
19. Seaberg MD, et al. (2014) Tabletop nanometer extreme ultraviolet imaging in an extended reflection mode using coherent Fresnel ptychography. *Optica* 1:39–44.
20. Seaberg MD, et al. (2011) Ultrahigh 22 nm resolution coherent diffractive imaging using a desktop 13 nm high harmonic source. *Opt Express* 19(23):22470–22479.
21. Miao J, Ishikawa T, Robinson IK, Murnane MM (2015) Beyond crystallography: Diffractive imaging using coherent X-ray light sources. *Science* 348(6234):530–535.
22. Mangin S, et al. (2014) Engineered materials for all-optical helicity-dependent magnetic switching. *Nat Mater* 13(3):286–292.
23. Mathias S, et al. (2012) Probing the timescale of the exchange interaction in a ferromagnetic alloy. *Proc Natl Acad Sci USA* 109(13):4792–4797.
24. Rudolf D, et al. (2012) Ultrafast magnetization enhancement in metallic multilayers driven by superdiffusive spin current. *Nat Commun* 3:1037.
25. Center for X-ray Optics (1995–2010) X-ray interactions with matter: Optics. Available at [henke.lbl.gov/optical\\_constants/](http://henke.lbl.gov/optical_constants/).
26. Chen MC, et al. (2014) Generation of bright isolated attosecond soft X-ray pulses driven by multicycle midinfrared lasers. *Proc Natl Acad Sci USA* 111(23):E2361–E2367.
27. Pisanty E, Sukiasyan S, Ivanov M (2014) Spin conservation in high-order-harmonic generation using bicircular fields. *Phys Rev A* 90:043829.
28. Milošević DB (2015) High-order harmonic generation by a bichromatic elliptically polarized field: Conservation of angular momentum. *J Phys At Mol Opt Phys* 48:171001.
29. Becker W, et al. (2002) Above-threshold ionization: From classical features to quantum effects. *Adv At Mol Opt Phys* 48:35–98.
30. Milošević DB, Becker W, Kopold R (2000) Generation of circularly polarized high-order harmonics by two-color coplanar field mixing. *Phys Rev A* 61:063403.
31. Milošević DB, Becker W, Kopold R (2001) High-harmonic generation by two-color circularly polarized field mixing. *Atoms, Molecules and Quantum Dots in Laser Fields: Fundamental Processes, Conference Proceedings*, eds Bloembergen N, Rahman N, Rizzo A (Italian Physical Society/Editrice Compositori, Bologna, Italy), Vol 71, pp 239–252.
32. Milošević DB, Becker W, Kopold R, Sandner W (2001) High-harmonic generation by a bichromatic bicircular laser field. *Laser Phys* 11:165–168.
33. Hickstein DD, et al. (2012) Direct visualization of laser-driven electron multiple scattering and tunneling distance in strong-field ionization. *Phys Rev Lett* 109(7):073004.
34. Milošević DB, Becker W (2000) Attosecond pulse trains with unusual nonlinear polarization. *Phys Rev A* 62:011403.
35. Hernández-García C, et al. (2010) High-order harmonic propagation in gases within the discrete dipole approximation. *Phys Rev A* 82:033432.
36. Milošević DB (2015) Generation of elliptically polarized attosecond pulse trains. *Opt Lett* 40(10):2381–2384.
37. Popmintchev T, et al. (2009) Phase matching of high harmonic generation in the soft and hard X-ray regions of the spectrum. *Proc Natl Acad Sci USA* 106(26):10516–10521.
38. Valencia S, et al. (2006) Faraday rotation spectra at shallow core levels: 3p edges of Fe, Co, and Ni. *New J Phys* 8:254.
39. Oppeneer PM (2001) Magneto-optical Kerr spectra. *Handbook of Magnetic Materials*, ed Buschow KHJ (Elsevier, Amsterdam), Vol 13, pp 229–422.
40. Stöhr J, Siegmann HC (2006) *Magnetism: From Fundamentals to Nanoscale Dynamics* (Springer, Berlin).
41. Pretorius M (1999) Magneto-optische Effekte mit linear polarisierter Synchrotronstrahlung im Bereich der 3p-Absorptionskanten der 3d-Übergangsmetalle Fe, Co und Ni. PhD thesis (Universität Hamburg, Hamburg, Germany). German.
42. Höchst H, Rioux D, Zhao D, Huber DL (1997) Magnetic linear dichroism effects in reflection spectroscopy: A case study at the Fe  $M_{2,3}$  edge. *J Appl Phys* 81:7584–7588.
43. Prieto JE, Heigl F, Krupin O, Kaindl G, Starke K (2003) Magneto-optics of Gd and Tb in the soft X-ray resonance regions. *Phys Rev B* 68:134453.
44. Prieto JE, Heigl F, Krupin O, Kaindl G, Starke K (2002) Prediction of huge X-ray Faraday rotation at the Gd  $N_{4,5}$  threshold. *Phys Rev B* 66:172408.
45. Takayama Y, et al. (2002) Magnetic circular dichroism of X-ray emission for gadolinium in 4d–4f excitation region. *J Phys Soc Jpn* 71:340–346.
46. Starke K, et al. (2001) X-ray magneto-optics in lanthanides. *Phys Rev Lett* 86(15):3415–3418.
47. Haskel D, et al. (2001) Enhanced interfacial magnetic coupling of Gd/Fe multilayers. *Phys Rev Lett* 87(20):207201.
48. Tripathi A, et al. (2011) Dichroic coherent diffractive imaging. *Proc Natl Acad Sci USA* 108(33):13393–13398.
49. Pérez-Hernández JA, Roso L, Plaja L (2009) Harmonic generation beyond the strong-field approximation: The physics behind the short-wave-infrared scaling laws. *Opt Express* 17(12):9891–9903.
50. Hernández-García C, et al. (2013) Zeptosecond high harmonic keV x-ray waveforms driven by midinfrared laser pulses. *Phys Rev Lett* 111(3):033002.
51. Becker A, Faisal F (2005) Intense-field many-body S-matrix theory. *J Phys At Mol Opt Phys* 38:R1–R56.
52. Ammosov MV, Delone NB, Krainov VP (1986) Tunnel ionization of complex atoms and atomic ions in a varying electromagnetic field. *Sov Phys JETP* 64:1191–1194.
53. Center for X-ray Optics (2015) X-ray attenuation length. Available at [henke.lbl.gov/optical\\_constants/atten2.html](http://henke.lbl.gov/optical_constants/atten2.html).